University of Bath

Alternative formats
If you require this document in an alternative format, please contact:
openaccess@bath.ac.uk

Further Investigations into the Benefits and Challenges of Eliminating Port Overlap in Wankel Rotary Engines

Author, co-author (Do NOT enter this information. It will be pulled from participant tab in MyTechZone)

Affiliation (Do NOT enter this information. It will be pulled from participant tab in MyTechZone)

Abstract

In a previous study it was shown that a production vehicle employing a Wankel rotary engine, the Mazda RX-8, was easily capable of meeting much more modern hydrocarbon emissions than it had been certified for. It was contended that this was mainly due to its provision of zero port overlap through its adoption of side intake and exhaust ports. In that earlier work a preliminary investigation was conducted to gauge the impact of adopting a zero overlap approach in a peripherally-ported Wankel engine, with a significant reduction in performance and fuel economy being found.

The present work builds on those initial studies by taking the engine from the vehicle and testing it on an engine dynamometer. The results show that the best fuel consumption of the engine is entirely in line with that of several proposed dedicated range extender engines, supporting the contention that the Wankel engine is an excellent candidate for that role. Also, continued 1-D modelling of the zero overlap peripherally-ported engine has shown that a potential route to regain lost performance and better fuel economy is to turbocompound the engine.

While compounding using turbomachinery provides one direction for further work, a new concept is proposed which uses the conventional three-flank Wankel rotor in its two-lobe housing to provide a positive displacement compounder to enable zero overlap anywhere in the device. This will allow the potential to configure large unobstructive ports with unimpeded timing. This novel concept is discussed in the paper.

Introduction

The Wankel engine has significant potential as a range extender (REx) for plug-in series hybrid vehicles due to its low mass, high power density, excellent vibration characteristics, and potentially low cost (due to its having a low parts count in comparison to conventional 4-stroke engines), as discussed in earlier work [1]. However, not insignificant challenges lie in its emissions and, to a lesser extent, fuel economy. The reason why the word "lesser"

qualifies the latter statement lies in the observation that the high-load fuel economy from Wankel rotary engines has been good enough to win fuel economy-based endurance races against then state-of-the-art 4-stroke engines e.g. at the 1991 Le Mans 24 hour race. Furthermore this was achieved against conventional engines in the last year of the World Sports Car Championship's Group C category, which was essentially a fuel consumption formula [2][1]. As a consequence of this success clearly elements of the fuel consumption map of the Wankel engine are satisfactory when compared to reciprocating engines. It is therefore reasonable that if the operating area of the Wankel engine can be constrained to be within this area of good fuel consumption then this would easily support its use as a REx provided it can still meet mandated emissions legislation.

The work reported here is a continuation of previous work conducted on a chassis dynamometer using a Mazda RX-8 vehicle [1] in which it was found that a Wankel rotary engine was capable of easily passing Euro 4 and 5 exhaust emissions regulations. While being able to meet the target was in itself not unexpected (since the former standard was what the vehicle was originally homologated for), the vehicle delivered hydrocarbon (HC) emissions 53.7% lower than the limit; the magnitude of its over-achievement was not expected given the historical reputation that the Wankel engine has had for high exhaust emissions levels.

Perhaps more remarkably, with HC emissions 59.7% lower than the Euro 6 limits, the vehicle delivered a greater level of over-achievement in HC emissions when tested against the current EU6 limits using the World-wide Light-duty Test Cycle (WLTC). This has a much longer and more aggressive form than the New European Drive Cycle (NEDC) for which the vehicle was originally developed. While the vehicle slightly failed in terms of oxides of nitrogen (NOx), there was more than enough headroom on HC to imagine the NOx limit being achievable via calibration effort. The previous work discussed the reasons for this excellent performance in terms of HC, and how the elimination of all port overlap was likely to be the primary reason, supported in the RX-8 through its 13B-MSP RENESIS engine's use of side intake and exhaust ports [3].

---

[1] The Group C regulations included a limitation on fuel tank size of 100 l and a maximum of five refuelling stops per 1000 km of racing (the minimum race length). Hence for a 1000 km race the cars effectively had a *total* limit of 600 l of fuel (this particular case

equating to 3.92 mpg US or 4.71 mpg Imperial), and logically the longer the race the incrementally better the fuel consumption had to become to finish.

This is unusual technology which not all Wankel engines can use depending on their rotor cooling configuration. Mazda adopted side intake ports relatively early for their production engines, although they kept the exhaust port in a peripheral location. However, while using side ports for the intake permits a significant reduction in port overlap, it cannot eliminate it. Using peripheral exhaust ports can, however, to the extent that the RENESIS engine effectively had -6° of port overlap in terms of eccentric shaft angle (ESA).

It should be noted that the 4-rotor engine that won Le Mans, the R26B, used both peripheral intake and exhaust ports [4], indicating that in itself this configuration is no impediment to offering good fuel consumption in a sizeable part of the operating map; this contention is discussed against the application of the engine as a range extender later in this work.

In the earlier work geometric studies were also conducted investigating the effect on the effective trapped compression ratio (CR) and expansion ratio (ER) of removing all overlap in a peripherally-ported Wankel engine [1]. This form of engine is the one which is being developed within the UK government-funded "ADAPT" project, and is capable of giving very high power outputs. It achieves this partly because of the very significant levels of port overlap inherent in the design when it is configured for conventional Otto cycle operation, which in turn gives it the ability to flow large amounts of air. The one-dimensional (1-D) engine performance studies in the previous work showed that such an approach was likely to result in greatly reduced performance, mainly because the effective CR and/or ER would have to be reduced massively to support the movement of the ports such that exhaust port closure (EPC) did not occur before inlet port opening (IPO).

Unlike in a reciprocating poppet-valve 4-stroke engine, it is not possible easily to increase effective CR or ER in the Wankel. This is because of the interaction of the generating radius (R), eccentricity (e), and housing width (B) with the acceptable apex seal leaning angle, the practical rotor flank cutout position and volume and how this in turn interacts with internal pumping across the minor axis of the troichoid housing. There is also an effect of surface area-to-volume ratio, a known challenge to control in the Wankel engine. While not specifically investigating it, the results of the earlier investigation into effective CR and ER might, however, logically suggest that turbocharging would likely be capable of offsetting this outright performance loss, and the authors have also conducted studies with a dedicated external Wankel expander (of the 1:2 geometry type, rather than the 2:3 type of the 4-stroke cycle Wankel engine) which could be used to regain expansion [5].

The present work builds on all of these earlier results by removing the engine from the vehicle used for drive-cycle testing and installing it on an engine dynamometer to record steady-state brake-specific results for emissions and fuel economy. This was done to verify the belief that in some areas of the operating map Wankel fuel consumption is comparable with that of a reciprocating 4-stroke engine. It was also done to help elucidate the reasons for the excellent emissions performance noted on the chassis dynamometer. This comprises the first section of this paper. To continue the relevance to peripheral porting, in the second section 1-D modelling of a compounded Wankel engine arrangement (using a production turbocharger turbine map) was also undertaken. In the final section a new arrangement of compounded Wankel engine is then proposed and discussed; preliminary studies have been started on this new concept using CFD. The resulting compounded arrangement is essentially one rotary version of a double compression-expansion

engine (DCEE), and its advantages over a single-stage Wankel engine are discussed in some detail.

Dynamometer Testing of a Mazda 13B-MSP RENESIS Engine

Engine description

The type of engine employed for the test work reported here is the Mazda 13B-MSP engine as described by Ohkubo et al. [3] (also known as the RENESIS). In this nomenclature, "13B" refers to the Mazda's base engine geometry in terms of R, e, and B, and "MSP" is an abbreviation for "multi-side port". The specifications of this engine are given in Table 1, taken from [3], where the quoted port timings are given before or after top dead centre (TDC) or bottom dead centre (BDC) as applicable.

Table 1: Mazda 13B-MSP "RENESIS" twin-rotor engine specifications, taken from [3].

Number of rotors	2
Radius, R (mm)	105
Eccentricity, e (mm)	15
Housing width, B (mm)	80
Capacity (cc)	1308
Geometric compression ratio (:1)	10
Port configuration	Side intake, side exhaust
Aspiration	Naturally-aspirated, variable
Fuel system	Indirect mixture preparation, port-fuel injected
Primary intake port opening (IPO) timing (°After TDC – ATDC)	3
Primary intake port closing (IPC) timing (°After BDC – ABDC)	65
Exhaust port opening (EPO) timing (°Before BDC – BBDC)	50
Exhaust port closing (EPC) timing (°Before TDC – BTDC)	3
Overlap (°ESA)	0 (effectively -6)

It should be noted that each chamber of the Wankel engine takes 1080° to complete the 4-stroke cycle, not the 720° taken in a

reciprocating engine, and the port timings in Table 1 reflect this. Also note that the 13B-MSP engine effectively has what is sometimes termed "negative" port overlap, the exhaust closing 6°ESA before the intake opens.

The particular unit used here had been rebuilt for chassis dynamometer testing by the ADAPT project as reported more fully in [1]. The RX-8 model was available in the UK market with two states of tune, and the ADAPT project had purposely sought a High Power variant fitted with a 6-speed manual transmission both for reasons of specific power and ease of testing with the Stahle robot driver at the University of Bath's rolling road facility. More complete details regarding this vehicle-based test programme can be found in [1]. After rebuild, the engine and exhaust system had been run in for 3000 miles (4827 km) in the vehicle. Full details on this, and the fuel and oil used during the process, are given in [1].

The engine was installed on the dynamometer together with the intake and exhaust systems used in the vehicle. The latter had to be modified slightly (in terms of the relative angles of the run post-catalyst) in order to fit in the test cell; however, the same pipework was used throughout. Because the engine had already been run-in while in the vehicle for the work [1] no further action was taken in this regard; as such its performance on the engine dynamometer was as close as possible to that which it gave on the chassis dynamometer. The engine loom was modified to enable operation on the standard controller, all test points discussed below therefore being gathered with it operating on the standard production engine management system (EMS) settings and on its standard operating maps.

Test cell equipment and instrumentation

Details of the test equipment used to record the performance and emissions of the 13B-MSP engine are given in Appendix 1. Instrumentation was attached to enable recording of engine speed, engine torque, fuel flow, etc., simultaneous pre- and post-catalyst emissions measurements being taken in order to ascertain catalyst efficiency and light-off criteria. Air flow was inferred from the fuel flow and the relative air-fuel ratio (AFR) λ.

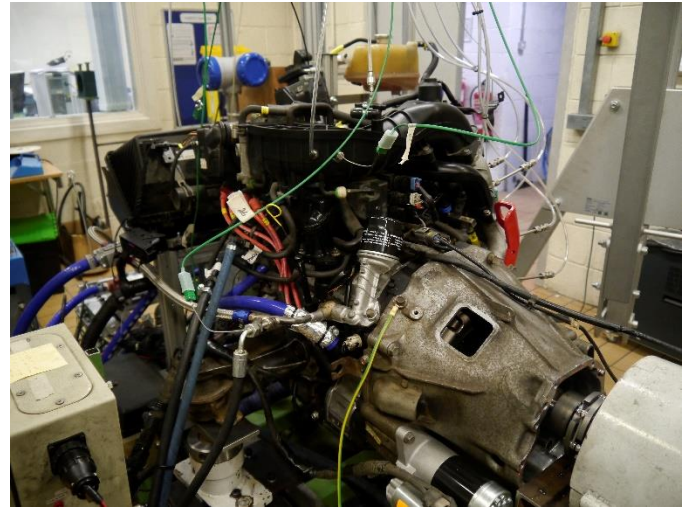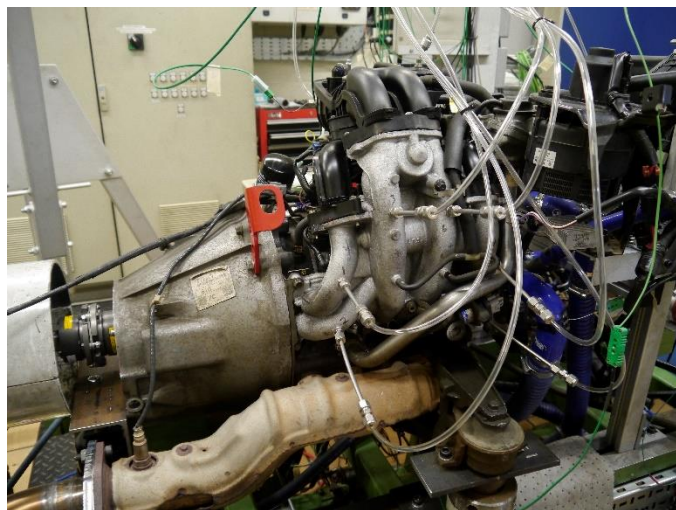Photographs of the engine as installed in the test cell are shown in Figures 1 and 2.

Fig. 1: Engine as installed on the test bed. Top: right hand side (i.e. intake and exhaust ports side); bottom: left hand side (i.e. ignition side)

Fuel and lubricant used

The fuel used was a 95 research octane number (RON) unleaded gasoline (ULG), this being the same fuel that was used for the chassis dynamometer testing described in [1]. More details on this fuel are given in Appendix 1.

The standard Mazda Dexelia Ultra 5W/30 fully-synthetic oil was used, this being the same as was used during running-in and dynamometer testing. The 13B-MSP engine has a total-loss lubrication system for the apex seals, with the oil being taken from the engine sump (the rotor and eccentric shaft plain bearings being pressure fed in a conventional manner from the same sump; the rotor is internally-cooled by the same oil). The engine oil level was checked every day and there was a hard cut-out associated with oil pressure in case the sump oil level fell too low and there was a danger of lubrication feed to the apex seals failing. This never occurred during testing.

Engine test procedure

All of the results were taken with the engine fully-warmed up and operating at steady state. The repeatability of engine performance was gauged daily by running controlled operating points of idle, 2000rpm/30Nm, 4000rpm/30Nm, and 4000rpm/60Nm, and checking for any drift in results. As mentioned above, the engine was operated using its standard EMS settings and operating maps, in order to gauge its performance in a production-standard configuration as it was homologated for road use.

In the following section the test results recorded for the 13B-MSP are reported up to 6000 rpm, essentially at 500 rpm intervals, and from zero to full load, at fixed brake mean effective pressure (BMEP) steps. At each speed and load point, represented in map form in Figure 2, three sets of data were taken which were then averaged. The reason for the spread in the data points in terms of BMEP is that there was some hysteresis in load depending on whether the engine was brought to the test point from a higher or lower speed; nevertheless the points shown were used to generate the maps of 13B-MSP engine performance shown below, in turn increasing their accuracy. From an operational point of view, in general the test

points were run starting from the lower left-hand corner of this map, to ensure the validity of the data with regards to the operating map in the vehicle, should any failure occur (see later).
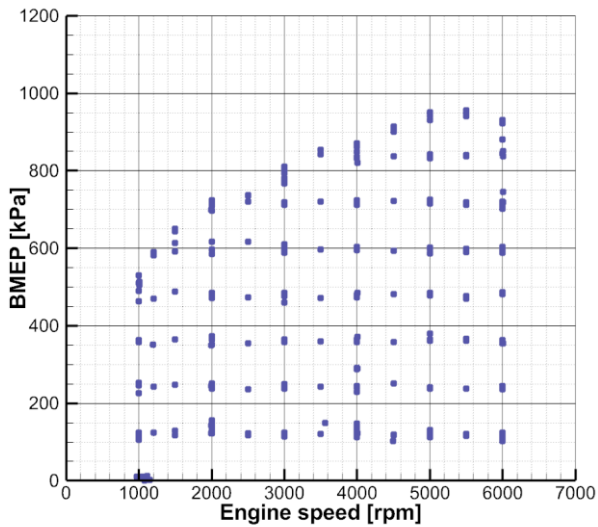

Fig 2: Speed and load test points

From analysis of the speed trace during the chassis dynamometer testing reported in [1] the range shown in Figure 2 amply covers the range of operation of the engine during both the NEDC and WLTC drive cycles; maximum engine speeds in those cycles were ~3750 and ~4400rpm respectively, with the maximum load tested here going up to wide-open-throttle (WOT).

Test results

A map of engine brake specific fuel consumption (BSFC) is presented in Figure 3. As stated, this was gathered using the standard EMS calibration and intake and exhaust systems, and here it can be seen that the best BSFC recorded is at 2000 rpm, 6.0 bar BMEP, where the engine gave a best individual point (of three, as discussed above) of 257.4 g/kWh. This represents a thermal efficiency of 33.9%. Furthermore, the data shows that there is a useful island of good BSFC close to this, but note that in general better such results are given at higher load in a similar manner to a reciprocating 4-stroke SI engine, although the magnitude of the change from low to high load will be discussed later.
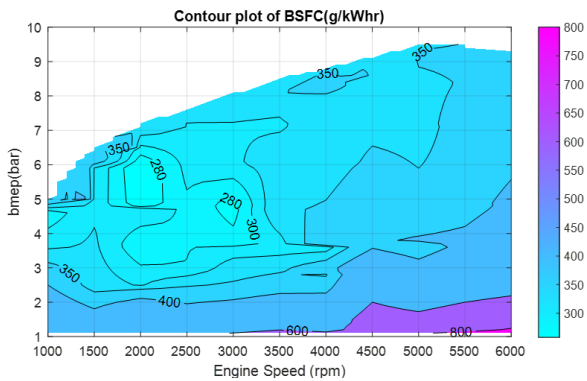
Fig. 3: Measured BSFC map for Mazda 13B-MSP twin-rotor engine

One important parameter having a bearing on BSFC and emissions is the AFR that the engine is operating under. This is shown in terms of λ in Figure 4. The engine operates near $\lambda=1$ for most of the measured range, as expected from the requirements of three-way catalyst (TWC) operation. At WOT enrichment only starts to occur at about 5000 rpm so it is interesting to note that the engine appears to operate with no real enrichment even at full load below this speed, i.e. that its knock control up to this point is not dependent on running rich. Equally it is accepted that, since all of this testing was performed using the standard EMS maps and settings, whether the ignition timing is retarded from its minimum advance for best torque settings for knock mitigation is unknown. Serious enrichment only really seems to start at about 6000 rpm.
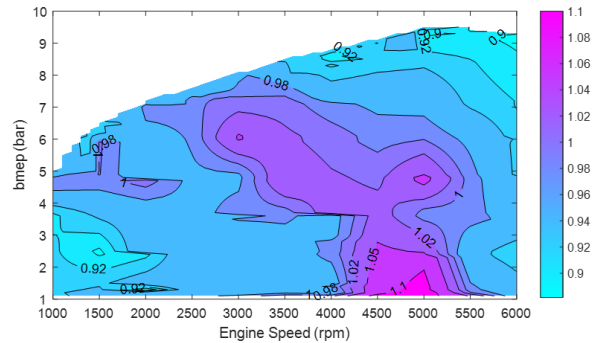

Fig. 4: Measured λ (relative AFR) map for Mazda 13B-MSP twin-rotor engine

With the engine operating on its standard settings, the measured maps for engine-out total HCs (THCs), carbon monoxide (CO), and NOx are shown in Figures, 5, 6, and 7 respectively.
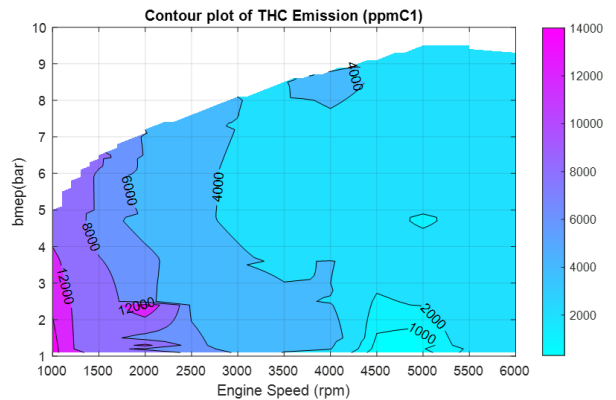

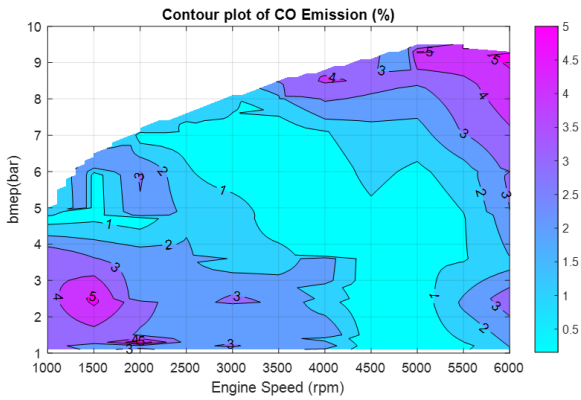Fig. 5: Measured engine-out HC map for Mazda 13B-MSP twin-rotor engine

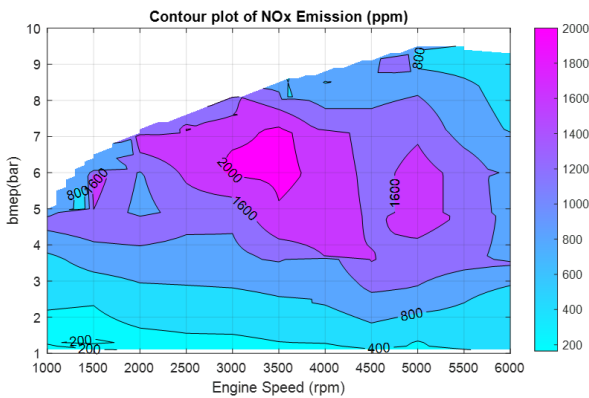Fig. 6: Measured engine-out CO map for Mazda 13B-MSP twin-rotor engine

Fig. 7: Measured engine-out NOx map for Mazda 13B-MSP twin-rotor engine

Considering these results and the test parameters, Figures 5 and 6 show that in general the HC and CO emissions are highest at low loads and speeds where the mixture is rich. However, above 4500 rpm and at high loads, even with the richer mixture, the observed emissions are to quite low. In the context of the current research this is an important finding since it shows that inherently the Wankel engine is capable of delivering good emissions performance and economy in large areas of its operating regime, as long as low speeds and loads can be avoided. This is discussed in relation to competing technologies for range extender engines later.

In Figure 7 NOx emissions are seen to be worst near the area of best efficiency. Since this is at higher load this is presumed to be at least partly due to gas dynamics, but this conjecture would need further investigation. Again, NOx emissions reduce as load and speed are further increased to an extent mimicking HC emissions, as well as at lower loads, all of which implies a good trade-off could be found for a range extender application.

All of this supports the findings in [1] where the vehicle that this engine was fitted to was found to give excellent emissions on the chassis dynamometer, including for drive cycles and associated limits considerably beyond what it was originally homologated for. From the prior and these results, fuel consumption (and the associated CO_2 emissions) when the Wankel engine is mated to a stepped transmission is its Achilles heel, not an inability to meet criteria pollutant emissions.

Figure 8 presents the engine-out oxygen concentration for the engine. The higher this value the worse the implications are for catalyst durability since, at an overall λ=1 operation in the exhaust, this implies increased exothermic combustion in the catalyst. However, a value of 1.2% is considered acceptable. This oxygen is logically the result of incomplete combustion only, the engine having zero port overlap and so no route for oxygen to short-circuit into the exhaust system.
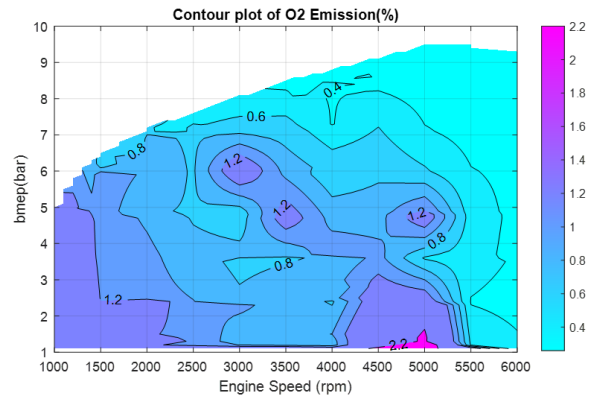

Fig. 8: Measured engine-out O_2 map for Mazda 13B-MSP twin-rotor engine

Catalyst efficiency was calculated from the engine-out and post-catalyst emissions measurements, and maps of these results are given in Appendix 2.

Like any engine installation an important consideration for any REx is its heat rejection. For the 13B-MSP this was estimated through flow rate measurement, temperature measurements in and out of the engine, and using the calculated specific heat capacities for the coolant and the oil reported in Appendix 3. Maps of the percentage heat rejection to coolant and oil are presented in Figures 9 and 10 respectively.
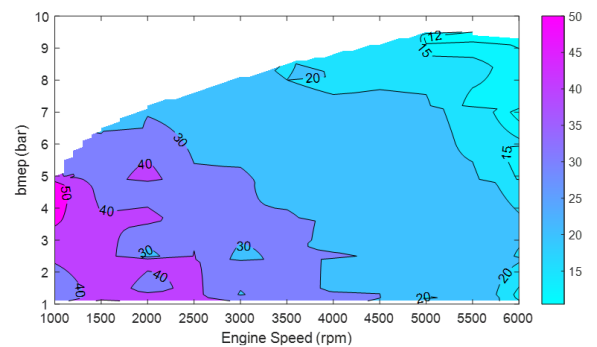

Fig. 9: Map of measured heat rejection to coolant as a percentage of total fuel input energy for Mazda 13B-MSP twin-rotor engine
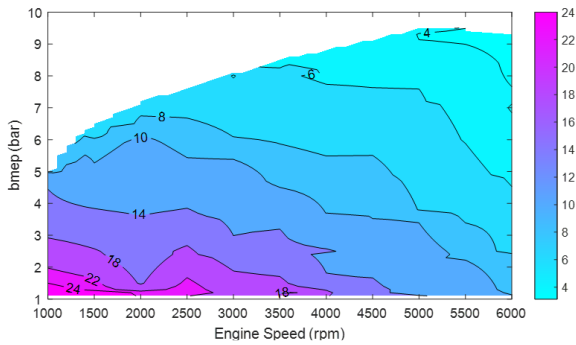
10/19/2016

Fig. 10: Map of measured heat rejection to oil as a percentage of total fuel input energy for Mazda 13B-MSP twin-rotor engine

Unfortunately the engine testing had to be curtailed because of a power take-off failure, but not before the results presented here had been taken. It had been hoped to be able to go fully up to maximum power and so to obtain a full operating map. Fortunately the engine was undamaged by this measuring equipment failure, and it is hoped to be able to take the remainder of the results at a later time.

Discussion of dynamometer results

In terms of the ADAPT project and the suitability of the Wankel engine for use as a REx, one can compare its performance firstly with those reported by Lotus and MAHLE for their dedicated 4-stroke spark-ignition (SI) reciprocating engine designs and secondly with the Wankel range extender concepts shown by AVL and FEV.

Of the two reciprocating engines, Lotus reported a best full-load BSFC of 241 g/kWh at a measured 36.8 kW at 3500 rpm maximum power point for their 3-cylinder engine [6], whereas MAHLE showed results in the region of 250 g/kWh for their 2-cylinder 30 kW unit, achieved between 2000 and 3000 rpm [7].

Both the dedicated Lotus and MAHLE REx engines had similar technology levels, illustrating that the same critical ratiocination of the two organization had led to a similarity in their products. In the interests of size, mass, and fuel economy they were both 2-valve-per-cylinder (2vpc) designs port-fuel injection (PFI) with reduced bearing sizes. The Lotus had a full-load BSFC range of between just over 248 and 241 g/kWh at 2000 rpm to 3500 rpm, this equating to almost 50% of the WOT power range, although in [6] they also showed values lower than this. While the first generation of MAHLE REx did not show results as low as the Lotus design it must be remembered that it was a smaller capacity engine and had a lower maximum power output. In comparison, MAHLE's latest hybrid engine (the "Dedicated Hybrid Internal Combustion Engine", or DHICE) has an increased technology level and with it better fuel consumption. While it still of a twin-cylinder, 2vpc configuration, it is now turbocharged with Miller cycle operation and uses jet ignition, albeit with PFI, and operates at much higher BMEP in the interests of mechanical efficiency, employing cooled exhaust gas recirculation for added knock suppression and efficiency while retaining the ability to operate at λ=1 to retain the use of a TWC. These additions ensure that it can operate over a much larger map than a simple range extender, and indeed it is intended to work as a prime mover under some circumstances; with all of these refinements its efficiency is quoted as 40% [8], which, using the same lower heating value (LHV) of 41.27 MJ/kg for the fuel used here, implies a best BSFC of 218 g/kWh.

10/19/2016

In comparison to these engines, with a best BSFC of 257.4 g/kWh the 13B-MSP has competitive fuel consumption and is not significantly worse than the original MAHLE REx, although it is noted that taking the best results in [6], the Lotus engine would have been approximately 10% better. The condition that the 13B-MSP gave its best result at, 2000 rpm / 6 bar BMEP, corresponds to 26.0 kW (34.9 bhp), so is broadly comparable with those engines. It also has the lower technology level of the Lotus and original MAHLE engines. With some of the technical refinements of the later MAHLE DHICE [8] and the benefit of a decade's further development effort, one might expect a modern Wankel engine to eclipse the two comparable dedicated REx reciprocating engines. This is presumably the rationale for Mazda developing such a range extender for its MX-30 electric vehicle [9].

As mentioned, both AVL [10,11] and FEV [12] have shown dedicated Wankel range extender engines, and indeed AVL's extensive "FUEREX" project (undertaken with Audi [13]) led to their development of specific Wankel engine simulation module in their 1-D engine simulation code BOOST. This is the simulation code used in the ADAPT project, it having been compared with the more widely used "equivalent 4-stroke" approach using reciprocating 1-D simulation models in an early comparison project [14]. Significantly more information is available on the AVL unit, and in [10] its power and fuel consumption are listed at 15 kW at 5000 rpm and 260 g/kWh, whereas later in [11] they are given as 18 kW at 5000 rpm and 275 g/kWh (with this later document listing the electric power as 15 kW). It is therefore assumed that, if these values apply to exactly the same engine specification, the best BSFC in [10] corresponds to 83% load (this being the ratio of power outputs, i.e. 15/18). In either case, the AVL engine had less design power than the Lotus and MAHLE engines, and at 254 cc it has a slightly larger capacity than the Advanced Innovative Engineering (AIE) 225CS Generation 2 engine that is the focus of the work within the ADAPT programme (see below, but which in [5] gave a best BSFC of 295 g/kWh at 3750 rpm, WOT). Nonetheless, the fuel consumption of the AVL is in the same region as that of the Mazda 13B-MSP tested here, despite its having a smaller displacement per rotor. It is also interesting to note that the 15 kW value equates to 7.1 bar BMEP, higher than the 6 bar for the tested best BSFC load for the Mazda 13B-REW reported here.

The AVL was a fully peripherally-ported engine, which may go some way to explaining why both its speed and load at best BSFC were higher than for the Mazda engine tested here. Nevertheless, given the difference in operating conditions, it can be contended that Wankel engines in general can give fuel consumption acceptable for range extender use.

Figure 11 shows a BSFC versus load plot at various constant engine speeds for the 13B-MSP, the lines effectively being slices through the data presented in Figure 4. Here it can be seen that the engine has quite large areas where it is under 300 g/kWh, and generally the best values are recorded at 2000 rpm between 4 and 6 bar BMEP. This is clearly where one would want to operate the engine should any hybrid system be attached to it. Also of interest on Figure 11 is that at the lowest speed shown of 1000 rpm, the BSFC worsens much more rapidly than for the other speeds. This is likely due to the disadvantages of the Wankel engine in terms of the surface area-to-volume ratio of its combustion chamber allowing significant heat loss, in turn exacerbated by very low speed of the rotor (this being one-third that of the eccentric shaft). This issue will likely also be compounded by sealing grid leakage effects. In support of this interpretation of the BSFC v load response, the next highest speed

shown in the figure, 2000 rpm, shows some evidence of this, as does – just – the 3000 rpm line.
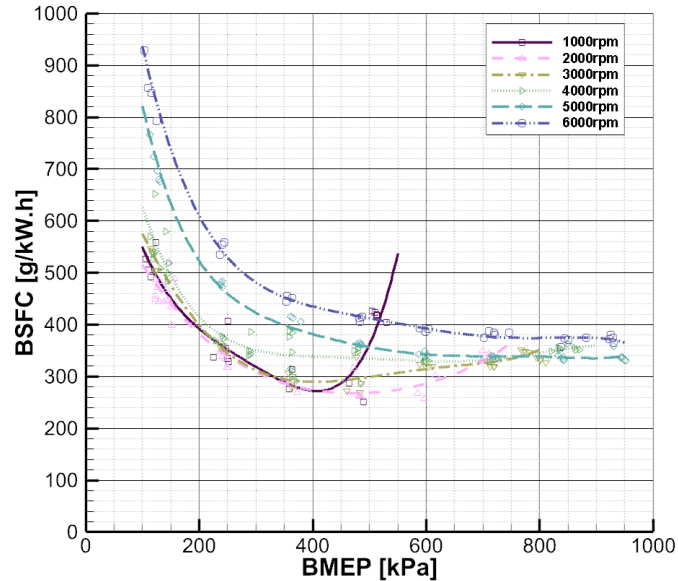

Fig. 11: BSFC versus BMEP for various constant speeds for Mazda 13B-MSP twin-rotor engine

However, it must be remembered that, like for a 2-stroke engine, one needs to double the BMEP of a Wankel engine to get the equivalent 4-stroke value. Comparing the 2000 rpm, 1 bar BMEP value to a scatter band of BSFC results at 2000 rpm, 2 bar versus engine capacity for similar-vintage 4-stroke engines (as shown in Figure 18 of [15]) one can see that the 13B-MSP is at a disadvantage, consuming as it does approaching 500 g/kWh here, compared to a value of 350 g/kWh for a 1.3 litre engine (and leaving aside discussions regarding Wankel engine swept volumes). The 13B-MSP value of 390 g/kWh at 2000 rpm, 2 bar is still over 10% worse than the typical best 4-stroke values at the time it was produced, although it is usefully towards the lower end of the range shown, and the exact technology levels of the engines plotted on the graph is unknown.

The BSFC map from the peripherally-ported AIE 225CS, being engineered as a range extender for the ADAPT project, is shown in Figure 12. This is of much smaller swept volume than the Mazda (about 70% less on a single-rotor basis) and so logically one would expect worse levels of BSFC. In the map one can plainly see the significant worsening of fuel consumption as the load is reduced, effectively to a much worse degree than one would expect for a 4-stroke SI engine with conventional throttling for load control. While it is accepted that the exact speed and load ranges covered are not the same as those shown in Figure 4, in comparison to the shape of the BSFC map obtained for the Mazda 13B-MSP there are some important differences. The iso-BSFC lines at low load in Figure 4 are at least turning up to give a best BSFC "eye" at low speed as the load and speed are increased. Also, the best BSFC point for the 225CS is at higher speed and load (especially in terms of the total load achievable at given speed) than the 13B-MSP, but generally one can say that for the three rotary engines for which the best BSFC data is available, they all appear to have their best BSFC values at a high proportion of the maximum BMEP achievable, i.e. at over 83%. Some of this will be due to the fact that they are all naturally aspirated, and therefore lacking the benefit of increased BMEP

offsetting friction that is one of the main benefits of engine downsizing with boosting [16], but for Wankel engines the friction is low for the reasons discussed in [1] and so this may not be significant here.
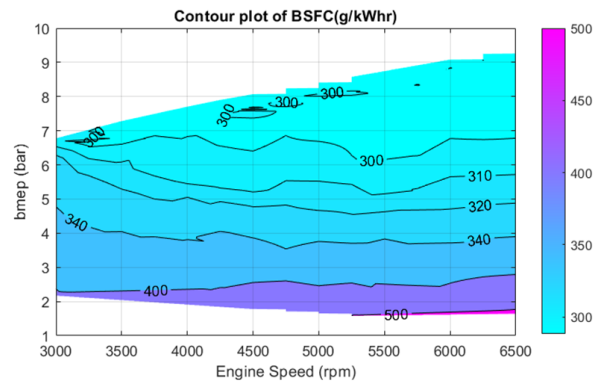

Fig. 12: Measured BSFC map for AIE 225CS single-rotor engine

Figure 13 presents the corresponding HC emissions data for the 225CS engine. In general the concentration of these emissions are of approximately twice as bad as the 13B-MSP (see Figure 5) and there are two very poor areas; the first corresponds to the best BSFC position, and is thought to be a result of the strong inlet pipe tuning for the engine (a known advantage of the Wankel engine). Although not presented here, this island also corresponds to the worst oxygen concentration in the exhaust. The second poor area is exactly where one would expect an engine with very significant port overlap to be: at low speed and low load. Hence, comparing the two sets of results for BSFC and HC emissions between the two engines, this shows the value of eliminating port overlap as far as this emission is concerned and that doing this can be expected to improve both HC emissions in general and fuel consumption at low speeds and loads in the Wankel engine, exactly as claimed by Mazda [3].
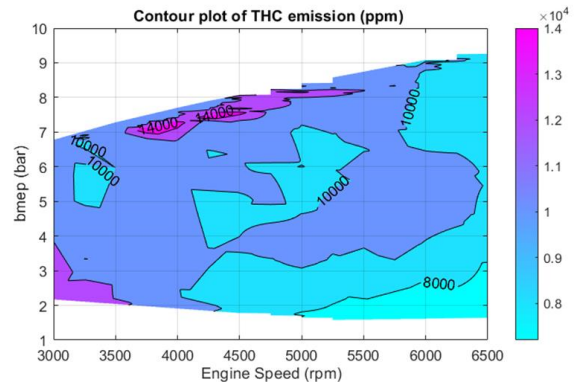

Fig. 13: Measured engine-out HC map for AIE 225CS single-rotor engine

To these points must be added the fact that that the currently-used Gen2 version of the 225CS engine uses a total-loss oil system as well as its self-pressurized air-cooled rotor cooling system (SPARCS), as discussed by Bailey and Lothan [17]. A future version of the engine, the Gen3, will adopt new proprietary technology to reduce its oil consumption. For this engine, target oil consumption is 10 cc per hour [18], which should bring it down to the levels of conventional automotive engines [19]. This new version will be tested at the University when it becomes available, at which point further

deductions can be made with regards to the HC emissions sources, i.e. from the fuel (itself arising either from incomplete combustion or unburnt fuel passing through during overlap) or unburnt oil.

One final point to make is that the magnitude of the BSFC change in the operating map from low-to-high load for Wankel engines is in general much greater than for conventional reciprocating 4-stroke engines. The magnitude of this can be determined from Figure 4, where below 2000 rpm and at 1 bar BMEP the BSFC is ≥ 450 g/kWh, rising to over 800 g/kWh at 6000 rpm. The values improve markedly by doubling the BMEP to 2 bar, and at this load are broadly in line with those reported for the 225CS engine reported in Figure 12. Still, it can be deduced that operating Wankel engines at higher loads is desirable to minimize the effect of poor fuel economy due to charge loss past the sealing grid, the increased proportion of heat losses at low speed due to the poor surface area-to-volume ratio, and in the case of high-overlap peripherally-ported engines the loss of unburnt charge due to short-circuiting to the exhaust.

In summarizing this section it has been shown that if Wankel engines can be operated away from regions where they are known to have very poor fuel economy (essentially, at the lightest loads, which unfortunately is where light-duty vehicles with stepped-ratio gearboxes tend to be driven in the real world) then they can be made to return competitive fuel consumption values, regardless of whether they are peripherally- or side-ported. This observation is wholly reinforced by the fact that Mazda's peripherally-ported R26B engine won Le Mans while being fuel-limited, as discussed above [2,4]. As such it is believed that this work validates the use of the Wankel engine as a range extender, as chosen by the ADAPT project. Eliminating port overlap might be expected to improve the area of the best BSFC region, and improve low speed and load behavior. This in turn extends the area of acceptable fuel consumption downwards, and from the work conducted both here and in [1] also permits extremely competitive exhaust emissions in vehicle.

The next section will discuss one option to regain performance and maintain economy in a peripherally-ported engine where overlap has been removed completely: turbocompounding.

Turbocompounding the peripherally-ported Wankel engine with zero port overlap

The foregoing section provides insight into the benefits of port overlap elimination in Wankel engines, especially with regards to applications in which their operation can be constrained to avoid very poor efficiency areas of the speed and load map. In the previous publication [1] a means of doing this was investigated in terms of its impact on engine performance, i.e. moving the ports so that an entire rotor flank can be between the EPC and IPO port timing edges. Figure 14 (reproduced from [1]) shows what is meant by this in schematic form.
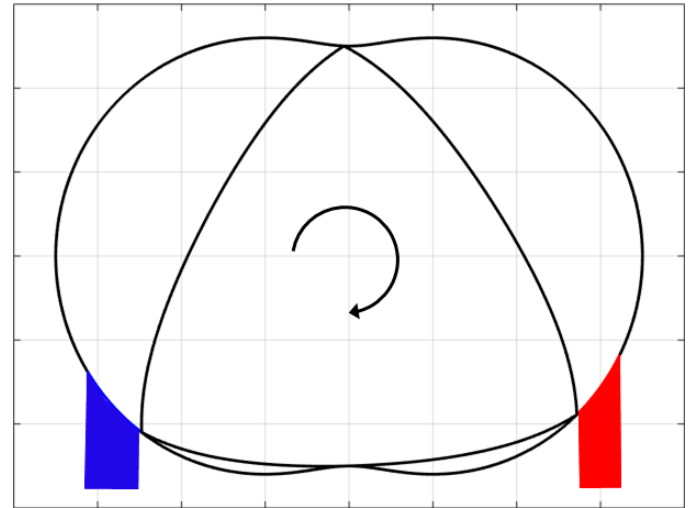

Fig. 14: Schematic representation of arrangement of intake (to left, in blue) and exhaust ports (to right, in red) for a zero overlap peripherally-ported Wankel engine

In the earlier work it was shown that rotating the ports clockwise around the housing (using the layout shown in Figure 14) gave a Miller-cycle effect, while swinging them anti-clockwise gave an "anti-Miller" effect. The representation of the port positions in Figure 14 is effectively for a conventional Otto cycle port timing. However, using the base AIE 225CS engine's geometry, this resulted in a reduction in compression ratio (CR) from a trapped 8.5 to approximately 5.5[2], with a concomitantly deleterious effect on fuel economy [1]. Also in that work the impact on the original engine torque of changing the port timings as a function of the ratio of ER/CR was shown. This work builds on that by expanding the model and applying turbocompounding to the engine using as its starting point the port timings found in [1] to offer the least reduction in engine torque – the so-called conventional Otto cycle port timing.

1-D Model development and investigation

Model implementation and charge cooling

Continuing the work by Turner et al. [1], the model was expanded to understand the impact of turbocompounding with chargecooling. As stated above an ER/CR ratio of 0.92 was chosen as the focus of the charge-cooling and turbocompounding studies because from the previous investigation this is where the reduction in brake torque was least affected. All other aspects of the model were retained from the previous work, to facilitate direct comparison. The modelling software used was AVL BOOST, since that is the only 1-D engine simulation package with a dedicated Wankel modelling domain, the value of which versus "equivalent 4-stroke" approaches was discussed by Peden et al. [14].

Here the initial investigation considered a simplified supercharger model (see Table 2), alongside an idealized charge air cooler (CAC) (see Table 3). It must be noted that the selected parameters are only

---

[2] Note that in all cases the geometric CR of the 225 CS remains at 9.6, as discussed in the earlier work [1].

indicative of a desired charging solution; further studies could look to implement a full supercharger performance map.

Pressure ratio (:1)	1.4, 1.5, … 1.9, 2.0, 2.25, 2.5, 3.0, 3.5, 4.0
Isentropic efficiency (%)	70
Mechanical efficiency (%)	97
Reference pressure (bar)	1
Reference temperature (°C)	30
Mechanical drive efficiency (%)	100

Reference mass flow (kg/s)	0.027979
Reference inlet air temperature (°C)	73
Reference inlet pressure (bar)	1.4
Target pressure drop (bar)	0.138
Coolant temperature (°C)	30.9
Target effectiveness (%)	85%
Total air cooler volume (l)	5
Inlet collector volume (l)	0.5
Outlet collector volume (l)	0.5
Length of cooling core (mm)	200

Impact of boost pressure on modified port arrangement

Figure 15 shows the implementation of the simplified charge cooling solution. The port timings and instantaneous chamber volumes are shown in Figure 16. The associated impact of boost pressure on the 0.92 ER/CR port arrangement was investigated by varying the supercharger pressure ratio for a given engine speed at full load. This is shown in Figure 17, where the supercharger pressure ratio was varied from 1.4 to 4.
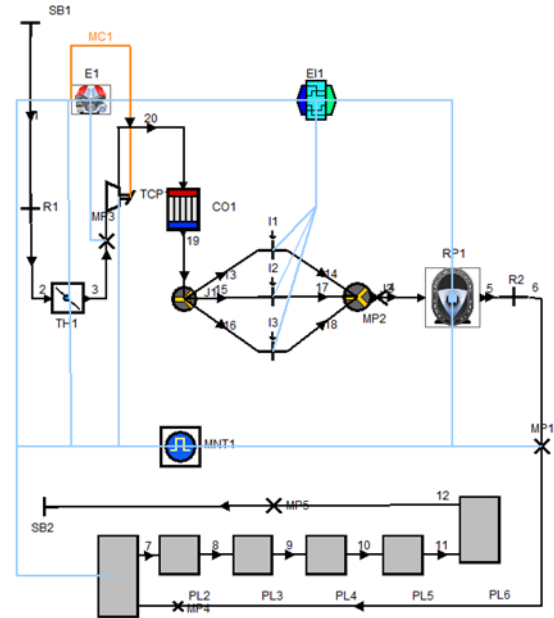

Fig. 15: AVL Boost 1-D simulation schematic of AIE 225CS Wankel rotary engine with supercharger (marked as TCP) and charge-air cooler (marked as CO1)
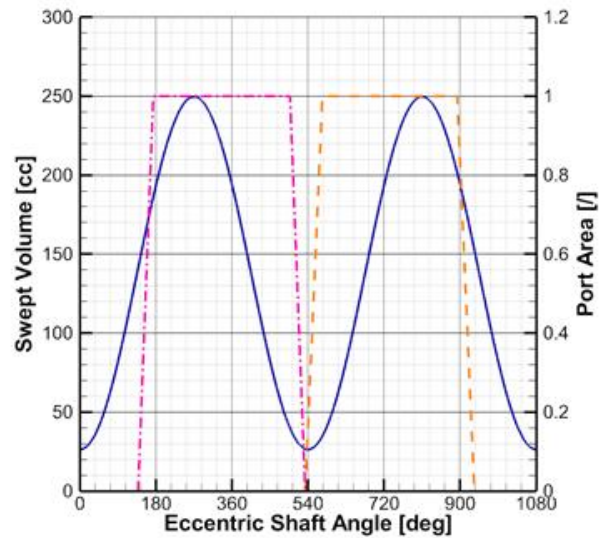

Fig. 16: Illustration of zero overlap port timing for the baseline case, maintaining an ER/CR ratio of 0.92. Also shown is the 225CS volume change with respect to ESA. (Swept volume in blue, intake port area representation orange dash, exhaust port area representation pink dash-dot.)

The simulation results in Figure 17 show that a boost pressure of at least 0.25~1.0 bar (gauge) (depending on engine speed) would be necessary to recover the BMEP lost as a result of the reduced CR and ER arising from the zero overlap porting arrangement. As expected, this results in a significant increase in fuel consumption of the order of 13–60% compared to the original validated 225CS 1-D simulation, as shown in Figure 18. In order to mitigate this negative impact, it was decided to implement a waste heat recovery system in the form of a compounder, which will be discussed in the next section.
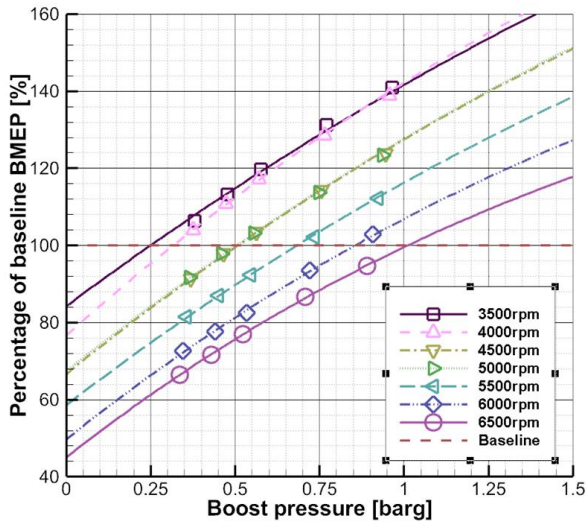
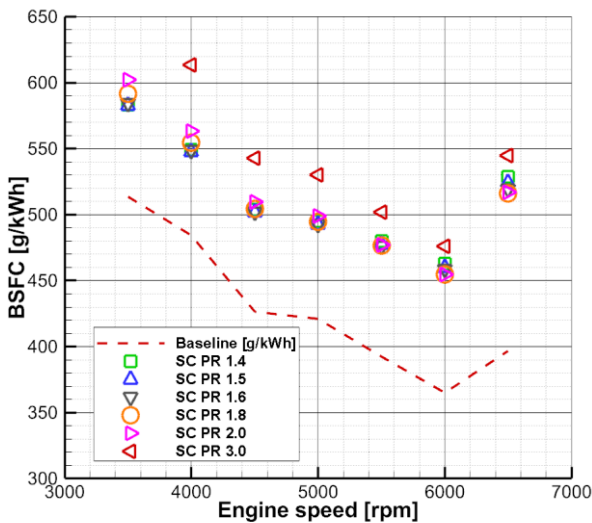Fig. 17: Percentage of baseline BMEP with respect to boost pressure (bar gauge) for different engine speeds

Fig. 18: Predicted BSFC at five fixed compressor pressure ratios, with reference to the simulated baseline 225CS engine performance

Improving system MEP through turbocompounding

Peripherally-ported Wankel engines have historically been known for high levels of exhaust energy, particularly when configured with an exhaust port that opens early relative to the geometric expansion of the rotor chamber. This suggests an opportunity for significant levels of exhaust energy recovery by placing an expander in the exhaust gas flow, as investigated in [5]. Furthermore, developments in electrified high-speed turbomachinery [20,21,22,23] have revealed the possibility of electric turbocompounding, promoting the idea of integrating an electrically turbocompounded Wankel engine into a hybrid electric vehicle as a REx, as well as the potential

electrification of the intake air charging device. This concept was investigated using the constructed model.

Initially the turbocompounding system model relied on a simplified orifice representation of a turbine, however this did not always lead to converged simulations. Following discussions with Mitsubishi Turbochargers, a production turbocharger map was obtained which was matched to the predicted exhaust flow conditions. The turbocompounding turbine sub-model now employs measured performance data for a Mitsubishi Turbocharger TD015 series turbine of 31.5mm diameter.

In terms of adapting this to the model, the turbocompounder was connected to the eccentric shaft via a fixed mechanical link, with an initial drive ratio of 15.4:1 and 100% mechanical efficiency. Later investigations will look into implementing a variable-ratio drive or electrical coupling (as used in Formula 1), which will account for both variations in the turbocompounding system and employ representative efficiencies. The exhaust system downstream of the turbine was simplified to a simple pipe geometry and the exhaust system boundary updated to a fixed pressure of 1.7 bar (absolute) to replicate a high flow after treatment system. The new system is shown in Figure 19. Since this is a value fixed across the reported speed range, this will tend to penalize performance below maximum speed; these factors should be borne in mind when interpreting the results reported later.
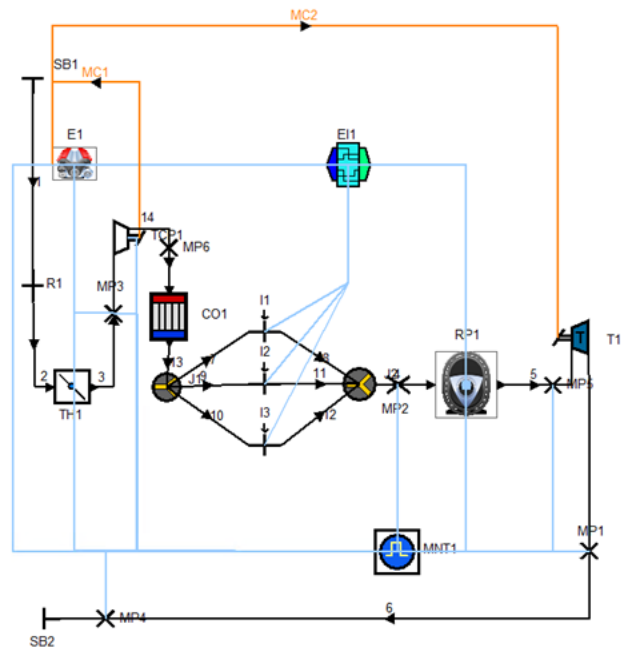
Fig. 19: AVL Boost model schematic incorporating turbocompounding machinery

With the real turbine map integrated into the model, the simulation was run in two hardware conditions, "supercharger only" (represented by Figure 15) and with turbocompounding (as per Figure 19).

As with any investigation into turbocompounding the end goal is to gauge the possibility to generate more work from the turbine than the work required to run the supercharger and to add this to the engine output shaft power in order to increase power and reduce fuel

consumption. Initially this outcome was unsuccessful: Figure 20 shows that while the additional work from turbocompounding versus the supercharged condition, termed the "ancillary mean effective pressure" (AMEP), reduced, net surplus work was not achieved.

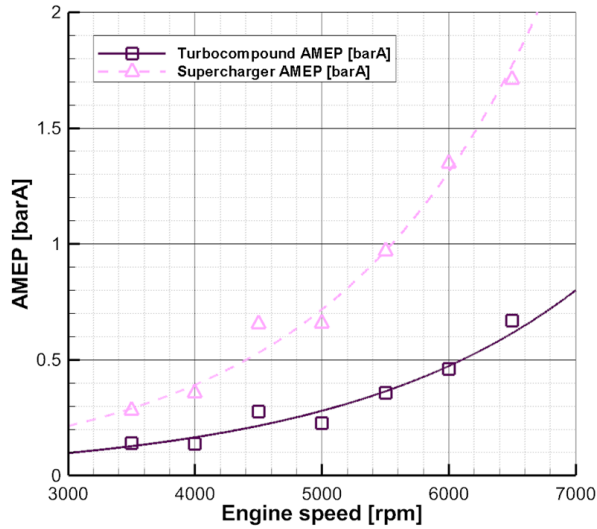Fig. 20: Ancillary mean effective pressure (AMEP) of Wankel rotary engine model with supercharger fitted (pink triangles) and supercharger plus turbocompound turbine (purple squares) at comparable system BMEP. Positive AMEP indicates parasitic loads on the system

While it should be remembered that the caveat of fixed drive ratio and fixed exhaust back pressure reported above apply, what can be seen is that AMEP increases with engine speed, and so making these two factors better would definitely be expected to improve performance at lower speeds.

At the simulated full load condition, turbine efficiency peaked at ~57% at 4500rpm and fell to ~38% at 6500rpm (both in terms of engine speed). This was not unexpected given the fixed engine to turbine speed ratio. Better matching of the turbine to the proposed hardware installation, especially in the context of e-turbocompound machinery, should yield better results. Another obvious factor is that this is a small engine with small turbomachinery attached to it, which is obviously a suboptimal condition with respect to best overall performance. However, the reduction in overall parasitic load was accompanied by a corresponding reduction in engine IMEP suggesting a level of sensitivity to exhaust back pressure which will need to be investigated further and lending credence to the observations made above.

After analyzing the results of this investigation an alternative cause of the reduction in IMEP was hypothesized: that this could to a significant degree be due to the reduction in trapped CR and ER caused by the zero overlap peripheral port timing adopted. This hypothesis was supported by the reported mass flows of both the exhaust and intake ports as shown in Figure 21.
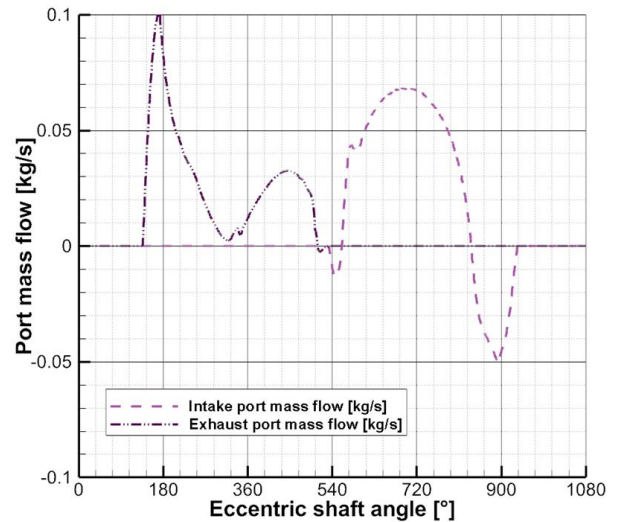

Fig. 21: Mass flow (in kg/s) at full load and 6000 rpm through the intake and exhaust ports relative to ESA for the original turbocompound model

The impact of intake port closing (IPC) timing on mass flow was then evaluated at the peak MEP condition of 6000rpm, full load, as shown in Figure 22. Advancing IPC timing in the cycle had two benefits: backflow was reduced with negligible impact on positive mass flow, causing more mass to be retained in the chamber to increase load directly, and the trapped compression ratio of the engine increased at the same time. While further data related to this parametric study is reported in Appendix 4, it can be seen in Figure 22 that for a fixed supercharger pressure ratio of 1.98 (the ratio required to achieve baseline torque with original port timing) advancing the intake port closing position beyond 80 degrees of ESA had a detrimental impact on engine IMEP.
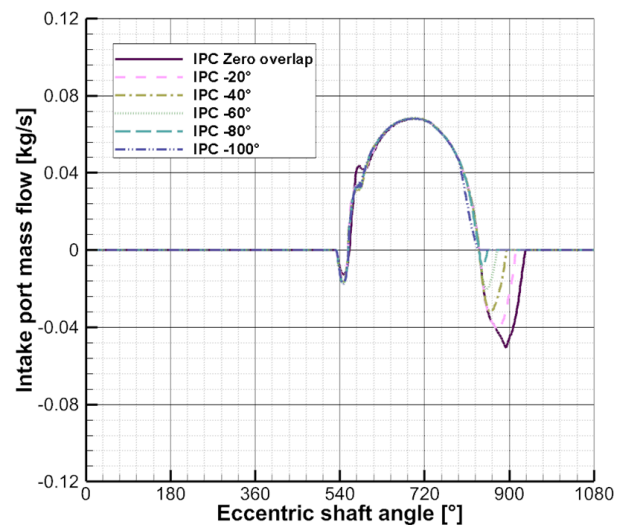

Fig. 22: Effect of advancing IPC timing on mass flow at 6000rpm, full load. IPO timing fixed at 7°BTDC (i.e. 533° ESA) throughout, while IPC timing was advanced in increments of 20° ESA

Exhaust port opening (EPO) timing was investigated in a similar manner. Figure 23 shows that for the original zero overlap timing the exhaust port mass flow separated into two distinct phases, an initial blowdown peak followed by a second distinct peak displacement flow. Again, a parametric study was conducted with EPO timing retarded in 20° increments of ESA, with the results shown in Figure 23. Delaying EPO had the effect of blending the two peaks of exhaust mass flow together. For this study, peak engine IMEP occurred at an EPO of plus 60° ESA versus the original zero overlap timing, with the corresponding increase in ER shown in Appendix 4.
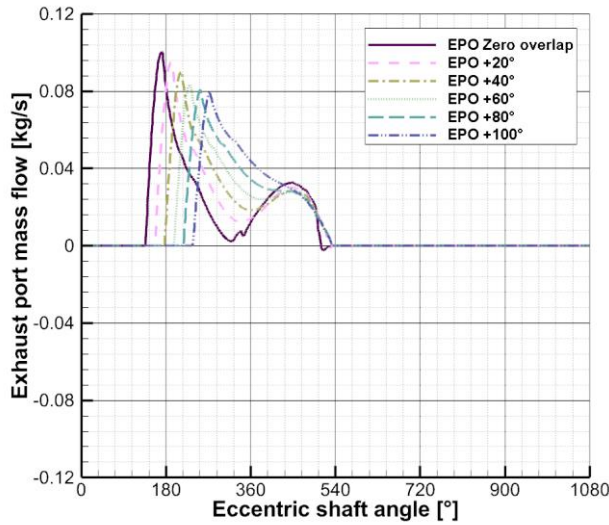
EPO (°BBDC)	69	133	73
EPC (°ATDC)	57	-7	-7
Duration (°ESA)	396	396	336
Chamber volume @ EPO (litres)	0.216	0.141	0.212
Trapped ER (:1)	8.20	5.35	8.05
ER/CR	0.96	0.92	0.90

Fig. 23: Effect of retarding EPO timing on mass flow at 6000rpm, full load. EPC timing fixed at -7° ATDC (i.e. 553° ESA) throughout, while EPO timing was retarded in increments of 20° ESA

It must be noted that in these studies on port timings, while port timing itself was modified, port flow coefficients and port area were assumed to remain constant throughout. This would be another area for investigation in any continuation of this work.

A final study of supercharger pressure ratio was investigated with the port timings reported in Table 4, these being selected to maximize engine IMEP from the previous individual investigations, i.e. they do not represent timings obtained from a joint parametric study. Figure 24 shows that under these conditions a supercharger pressure ratio of 1.32 was found to recover most of the lost performance due to the delayed IPO, with intake backflow almost eliminated.

Table 4: Optimized zero overlap port timing for turbocompounded engine system. Negative values for EPC indicate degrees before TDC

Parameter	Baseline	Original Zero Overlap	IPC and EPO Optimized for IMEP
IPO (°BTDC)	71	7	7
IPC (°ABDC)	60	124	44
Duration (°ESA)	401	401	321
Chamber volume @ IPC (litres)	0.223	0.152	0.235
Trapped CR (:1)	8.50	5.79	8.95

Fig. 24: Total system BMEP of the baseline model compared to the compounded system with zero overlap peripheral port timing and updated EPO and IPC timing (see text)

With the updated port timing and reduced supercharger pressure ratio Figure 25 shows that net AMEP fell and above 5500rpm the combined turbocompound ancillary load provided a net contribution to total system MEP; Figure 26 shows that at the same time the total system BSFC also fell but did not improve over baseline performance. It is expected that further work on turbine matching would improve this outcome, and additionally as mentioned above the fixed exhaust system boundary pressure of 1.75 bar (absolute) likely compromises the performance of the charging devices below 6000 rpm, so that there would possibly be a benefit in future simulations utilizing an alternative arrangement.

10/19/2016

Fig. 25: Ancillary MEP (AMEP) comparison at comparable BMEP. Zero overlap supercharged system, zero overlap turbocompound system, and turbocompound system with updated IPC and EPO timing (see text)

Fig. 26: Comparison of brake specific fuel consumption for baseline system model, zero overlap supercharged system, and turbocompound system with updated IPC and EPO timing (see text)

A final point of considerable interest in Table 4 is that with the revised port timings the CR is actually higher than the original, conventional system, and the ER is almost as great; therefore the ER/CR ratio is nearly the same. This is because pressurized air is now being supplied to the engine, and at equivalent BMEP less angle-area is therefore needed. Further optimization of all port timings could yield yet further benefits on a system level.

Future model development

The impact of boost pressure on gasoline heat release is well established for reciprocating 4-stroke engines [19] but this is not necessarily the case for the Wankel rotary engine with its unique combustion chamber arrangement. A clear avenue for future study is to focus on the development of this aspect of the model, either through validation against direct testing, which is difficult for the Wankel engine with its continuously-moving combustion chamber [24], or via CFD simulation. Improved heat release curves should also allow a further correlation loop of wall heat loss coefficients improving model validation. Throughout the work reported here the same heat release profile has been used out of necessity.

With a new baseline established several new investigation streams can be investigated, the most significant of which would be the implementation of a realistic matched compressor map and electrically assisted turbocompound machinery and their associated efficiencies. It could also be used to investigate positive-displacement compounders (see later).

Initial simulation conclusions

The reported studies suggest a possible route forward for peripherally-ported Wankel rotary engines with zero overlap through the implementation of turbocompounding with modest levels of boost pressure. This combination will eliminate several issues with peripherally-ported engines, such as the high HC emissions and high oxygen concentration in the exhaust, while maintaining the benefits of peripheral ports in terms of simplicity and manufacturing.

As previously highlighted further development will be required to progress the model further, specifically better heat release functions, further supercharger and turbine mapping plus port and system boundary condition updates. It is believed likely that a high efficiency turbocompound arrangement could be deployed in conjunction with a zero overlap Wankel engine in an automotive REx application.

It should be noted that the small size of AIE 225CS engine used in this study could be working against the aims of the investigation, since implementing turbocompounding on an engine with a small swept volume of 225cc does not lend itself to using high efficiency turbomachinery. As discussed in the next section a positive displacement device may well be a better choice in this application.

Finally, the CR and ER of the engine can be largely recovered by the approach taken here, and hence a full optimization of all port timings would be beneficial.

The two-stage compounded Wankel engine with zero overlap

Following the above investigations a new concept has been created in order to better match the compounding arrangement to smaller engine sizes, to remove port overlap throughout the resulting engine, and to reduce the loss in overall compression ratio with moving the port timing edges. This is to compound the "normal" Wankel engine with a larger Wankel compressor/expander in the manner of the Rolls-Royce R1 and 2-R6 "Cottage Loaf" engines from the 1960s and early 1970s [25,26,27].
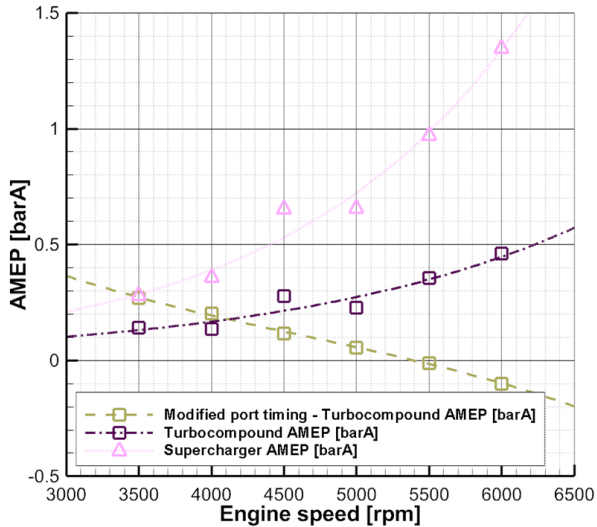
10/19/2016

The basic arrangement of this new concept is well-known from the Rolls-Royce engine, but that engine was intended to operate on the diesel cycle and was therefore not sensitive to port overlap in the same way. The specific novelty of the concept here is to adopt zero overlap port timings for the smaller, high-pressure (HP) Wankel device, in which combustion occurs, with the larger, low-pressure (LP) rotor being used to provide higher compression ratio and effective swept volume. The concept is shown as an initial CFD model in Figure 27.

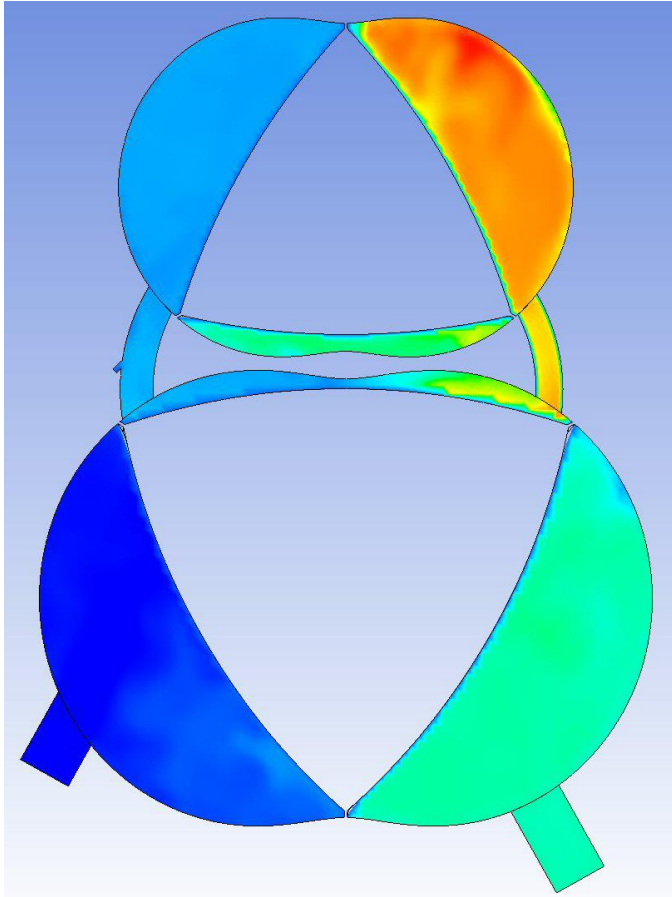Fig. 27: Concept of zero overlap two-stage compound rotary engine. The upper high-pressure rotor and lower low-pressure rotor rotate at the same speed and in the same direction, clockwise in this view. Note that in this CFD model the clearances between the rotor flanks and housings are not fully refined, that a semi-Miller intake port position is shown for the low-pressure rotor, and that a potential injector position is discernible in the transfer port on the cold side of the engine linking the two rotors' chambers

The resulting concept is essentially a form of double compression-expansion engine (or double-compression, double-expansion engine), such as is presently being investigated by KAUST and General Motors [28,29,30,31]. Indeed, the authors would contend that the Rolls-Royce design was the first such internal combustion application of the idea.

In the form discussed here, because combustion does not occur in the LP rotor, and gases never have to be passed across the minor axis, there is no need for rotor cutouts in that rotor and indeed they would degrade its function (note that these cutouts are not shown in the HP rotor in Figure 27). The approach of the LP rotor flank to the housing minor axis effectively eliminates port overlap in the LP

rotor, meaning very large port timings can be adopted to the benefit of performance. At the same time the HP rotor has no overlap through its port positioning.

An important further advantage is that there is effectively a reduced surface area in the HP rotor for any given LP rotor swept volume, reducing overall heat rejection versus the intake volume of the LP rotor. The higher-density combustion should accelerate the combustion rate over a larger, single-stage engine with the same performance as well. Furthermore, the two rotors rotate in the same direction and at the same speed, making it feasible to use a simple timing drive between the two (the Rolls-Royce engine used a gear drive comprising three gears in two meshes [25], but it is believed a belt drive would be just as feasible).

The LP rotor only ever sees much lower pressures than the HP rotor, so its configuration and sealing grid can be specifed to minimize friction in that area (for a conventional oil-cooled engine, for example, a single compression side seal would likely suffice). Other major advantages are that a CAC can be placed in the transfer duct on the cold side between the two rotors, and fuel injection can be positioned in that area as well, possibly improving mixture preparation while avoiding unburnt fuel carryover (through the zero overlap arrangement). The position of such a fuel injector is discernible in the cold-side transfer duct in Figure 27. Positioning fuel introduction here means it can also be a relatively low-pressure device, further saving cost and parasitic load versus a high-pressure direct-injection arrangement.

Finally, separate and switchable ports could be positioned around the periphery of the LP rotor, giving successively greater Miller timings. These would allow a degree of load control via port timing itself, to the benefit of reduced pumping work in the cycle.

Other configurations and concepts have been imagined (including the use of side ports for some, or indeed all, of the ports, for example), but they will not be discussed further here. CFD modelling on this particular concept is ongoing, with the intention of publishing results at a later date.

Summary/Conclusions

In an earlier paper the advantages of the elimination of port overlap in a Wankel rotary engine were investigated through the testing on a chassis dynamometer of a rebuilt Mazda RX-8 vehicle, whose 13B-MSP engine used side intake and exhaust ports to achieve this end. An initial 1-D modelling investigation in that work into how to apply the zero overlap approach to a peripherally-ported engine disclosed some of the challenges associated with that aim.

In the present work the engine from the vehicle that was originally tested was installed on a test bed and mapped for more detailed engine performance results which have been reported here. This was done to help understand the feasibility of the use of a Wankel engine as a REx for a plug-in series hybrid vehicle. At the same time addressing the challenges of significantly reduced compression and expansion ratios when adopting zero overlap port timings in a peripherally-ported engine was investigated using a turbocompounding approach. Accordingly, this investigation has shown:

- The best fuel consumption of the tested Mazda 13B-MSP Wankel engine was entirely in line with that reported for

various dedicated REx engines. These in themselves are much younger designs, and so the authors contend that the validity of adopting the Wankel engine as a REx is proved.

- The general fuel consumption of a peripherally-ported engine tested as part of the ADAPT project is in the same area as that of the 13B-MSP. This suggests that peripheral ports can be adopted for those applications.
- Unfortunately in the peripherally-ported engine the best BSFC position also results in high levels of unburned hydrocarbons. This suggests there is validity in investigating means of providing zero overlap in such engines.
- A turbocompounding investigation was conducted on a peripherally-ported engine using a validated 1-D model, coupled to a production turbocharger map. This suggested that engine performance can be fully recovered with optimized port timings, and that fuel consumption, while slightly worse in the modelling conducted, could probably be made as good as (if not better than) the original, although that assertion is unproven at present.
- The fact that turbocompounding was shown to be a feasible route forward for such a small base engine, which necessarily would have to employ very small turbomachinery, logically suggests that positive-displacement machines would be worth investigating in this application.
- A new form of compounded rotary engine, owing its basic concept to that of the Rolls-Royce "Cottage Loaf" engine but utilizing the zero overlap approach investigated here, has been proposed. This should give myriad advantages over a single-stage engine of equivalent LP stage swept volume, albeit at the expense of increased mechanical complexity.

The work reported here therefore shows a way forward for Wankel engines to be adopted either for use as a REx in a plug-in series hybrid vehicle or as a prime mover in hybridized ones. Further work is ongoing in several of these directions.

References

1. Turner, J.W.G., Turner, M., Vorraro, G., and Thomas, T.J., "Initial Investigations into the Benefits and Challenges of Eliminating Port Overlap in Wankel Rotary Engines", SAE technical paper 2020-01-0280, SAE 2020 World Congress, Detroit, Michigan, USA, 21st-23rd April, 2020, doi:10.4271/2020-01-0280.
2. https://en.wikipedia.org/wiki/Group_C, last accessed 15th November, 2020.
3. Ohkubo, M., Tashima, S., Shimizu, R., Fuse, S. and Ebino, H., "Developed Technologies of the New Rotary Engine (RENESIS)" SAE technical paper 2004-01-1790, SAE 2004 World Congress, Detroit, Michigan, USA, 8th-11th March, 2004, doi:10.4271/2004-01-1790.
4. Shimizu, R., Tadokoro, T., Nakanishi, T. and Funamoto, J., "Mazda 4-Rotor Rotary Engine for the Le Mans 24-Hour Endurance Race", SAE technical paper 920309, SAE 1992 World Congress, Detroit, Michigan, USA, 24th-28th February, 1992, doi:10.4271/920309.
5. Vorraro, G., Islam, R., Turner, M., and Turner, J.W.G., "Application of a rotary expander as an energy recovery system for a modern Wankel engine", I.Mech.E. Internal Combustion Engines and Powertrain Systems for Future Transport Conference, Birmingham, U.K., 11th-12th December 2019.
6. Turner, J.W.G., Blake, D., Moore, J., Burke, P., Pearson, R.J., Patel, R., Blundell, D.W., Chandrashekar, R.B., Matteucci, L., Barker, P., and Card, C.A., "The Lotus Range Extender Engine", SAE technical paper 2010-01-2208, SAE Powertrains, Fuels and Lubricants Meeting, San Diego, California, USA, 25th-27th October, 2010, and SAE Int. J. Engines 3(2):318-351, doi:10.4271/2010-01-2208.
7. Warth, M., Bassett, M., Hall, J., Korte, V., and Mahr, B., "Design and Development of the MAHLE Range Extender Engine", 20th Aachen Colloquium, pp. 845-869, Aachen, Germany, 10th-12th October, 2011.
8. Bassett, M., Cooper, A., Reynolds, I, Hall, J., Reader, S., and Berger, M., "MAHLE Modular Hybrid Powertrain", I.Mech.E. Internal Combustion Engines and Powertrain Systems for Future Transport Conference, Birmingham, UK, 11th-12th December 2019.
9. Mazda Europe, "Mazda rotary engine to return as EV range-extender", https://www.mazda-press.com/eu/news/2018/mazda-rotary-engine-to-return-as-ev-range-extender-/, last accessed 15th November, 2020.
10. Fischer, R., Fraidl, G.K., Hubmann, C., Kapus, P.E., Kunzemann, R., Sifferlinger, B., and Beste, F., "Range Extender Module - Enabler for Electric Mobility", ATZautotechnology Vol. 9 pp. 40-46, May 2009.
11. Sams, T. and Sifferlinger, B., "AVL Rotary Range Extender - A Rotary Engine Based Range Extender Concept", E-Mobility Conference 2013, Graz, Austria, 30th January, 2013.
12. "Plug-In E-Vehicle with and without Range Extender", FEV Spectrum, Issue 39, pp. 1-3, 2009, https://www.fev.com/fileadmin/user_upload/WhatWeDo/Electrical%20Systems%20and%20Electronics/Electric%20Vehicles-Plug-Ins2.pdf, last accessed 15th November 2020.
13. "Audi showcases cars' electrifying performance", Automotive Engineer, April 2010, p.49.
14. Peden, M., Turner, M., Turner, J.W.G., and Bailey, N., "Comparison of 1-D Modelling Approaches for Wankel Engine Performance Simulation and Initial Study of the Direct Injection Limitations," SAE Technical Paper 2018-01-1452, 2018, doi:10.4271/2018-01-1452.
15. Coltman, D., Turner, J.W.G., Curtis, R., Blake, D., Holland, B., Pearson, R.J., Arden., A. and Nuglisch, H., "Project Sabre: A Close-Spaced Direct Injection 3-Cylinder Engine with Synergistic Technologies to achieve Low CO$_2$ Output", SAE technical paper 2008-01-0138, SAE 2008 World Congress, Detroit, Michigan, USA, 14th-17th April, 2008, and SAE Int. J. Engines 1(1):129-146, 2009, doi:10.4271/2008-01-0138.
16. Turner, J.W.G., Popplewell, A., Patel, R., Johnson, T.R., Darnton, N.J., Richardson, S., Bredda, S.W., Jackson, R., Bithell, C., Tudor, R., Fernandes, J., Remmert, S., Cracknell, R., Lewis, A.G.J., Akehurst, S., Brace, C.J., Copeland, C., Martinez-Botas, R., Romagnoli, A. and Burluka, A.A., "Ultra Boost for Economy: Extending the Limits of Extreme Engine Downsizing", SAE technical paper 2014-01-1185, SAE 2014 World Congress, Detroit, Michigan, USA, 8th-10th April, 2014 and SAE Int. J. Engines 7(1):2014, doi:10.4271/2014-01-1185.
17. Bailey, N. and Lothan, L., "The Compact SPARCS Wankel rotary engine", JSAE technical paper 20154346, JSAE 2015 Congress, Yokohama, Japan, 20th-22nd May, 2015.
18. Bailey N., private communication, November 2020.
19. Heywood, J.B., Internal Combustion Engine Fundamentals, 2nd Edition, McGraw-Hill Book Company, New York, USA, 2018, ISBN 978-1-260-11610-6.
20. Cooper, A., Bassett, M., Hall, J., Harrington, A., Reader, S., Hartland, J., Harris, J., and Taylor, A., "HyPACE - Hybrid Petrol Advance Combustion Engine - Advanced Boosting System for Extended Stoichiometric Operation and Improved Dynamic Response", SAE technical paper 2019-01-0325, SAE

10/19/2016

2019 World Congress, Detroit, Michigan, USA, 9th-11th April, 2019, doi:10.4271/2019-01-0325.

21. Terdich, N., Martinez-Botas, R. F., Howey, D. A., Copeland, C. D., and Costall, A., "Off-road diesel engine transient response improvement by electrically assisted turbocharging", SAE technical paper 2011-24-0127, 10th International Conference on Engines and Vehicles, Capri, Naples, Italy, 11th-15th September, 2011, doi:10.4271/2011-24-0127.

22. Costall, A. W., Ivanov, R., and Langley, T. P. F., "Electric turbo assist as an enabler for engine downspeeding", in Proc. ASME Turbo Expo 2012, pp. 511–521, paper GT2012-68246, 2012.

23. Winward, E., Rutledge, J., Carter, J., Costall, A., Stobart, R., Zhao, D., and Yang, Z., "Performance testing of an electrically assisted turbocharger on a heavy duty diesel engine", in Proc. IMechE 12th International Conference on Turbochargers & Turbocharging, London, UK, May 2016, pp. 363–382.

24. Vorraro, G., Turner, M., and Turner, J.W.G., "Testing of a Modern Wankel Rotary Engine – Part I: Design of the Experiments, Development of the Software Tools and Measurement Systems", SAE technical paper 2019-01-0075, SAE 2019 Powertrain, Fuels and Lubricants Conference, San Antonio, Texas, USA, 22nd-24th January, 2019, doi:10.4271/2019-01-0075.

25. Feller, F., "The 2-stage rotary engine – a new concept in diesel power", Proc. Instn Mech. Engrs, 1970-71, Vol. 185 13/71, pp. 139-158, 1971.

26. Daniels, J.R., "Rolls-Royce make a Wankel", Autocar Magazine, 17th December, 1970, pp. 16-17.

27. Norbye, J.P., The Wankel Engine: Design, Development, Applications, Bailey Brothers and Swinfen Limited, Folkstone, UK, 1972, ISBN 0561001375.

28. Shankar, V.S.B., "Double Compression Expansion Engine: Evaluation of Thermodynamic Cycle and Combustion Concepts", Ph.D. thesis, King Abdullah University of Science and Technology, November, 2019.

29. Nyrenstedt, G., Alturkestani, T., Im, H., and Johansson, B., "CFD Study of Heat Transfer Reduction Using Multiple Injectors in a DCEE Concept", SAE technical paper 2019-01-0070, SAE 2019 Powertrain, Fuels and Lubricants Conference, San Antonio, Texas, USA, 22nd-24th January, 2019, doi:10.4271/2019-01-0070.

30. Andruskiewicz, P., Durrett, R., Gopalakrishnan, V., and Najt, P., "Dual-compression, dual-expansion piston engine assessment and optimization", International Journal of Engine Research, 10th October, 2019, available at: https://journals.sagepub.com/doi/10.1177/1468087419879609 , last accessed 15th November, 2020.

31. Andruskiewicz, P., Durrett, R., and Najt, P., "Low-load expander deactivation studies for a light-duty single-shaft piston-compounded engine", International Journal of Engine Research, 8th November, 2019, doi:10.1177/1468087419886501.

Contact Information

Dr James Turner
Professor of Engines and Energy Systems
Department of Mechanical Engineering
University of Bath
Claverton Down
Bath BA2 7AY
United Kingdom

j.turner@bath.ac.uk

Acknowledgments

Definitions/Abbreviations

1-D	One-dimensional
2vpc	Two-valves-per-cylinder
ABDC	After bottom dead centre
AFR	Air-fuel ratio
AIE	Advanced Innovative Engineering
AMEP	Auxiliary mean effective pressure
ATDC	After top dead centre
B	Housing width
BBDC	Before bottom dead centre

BDC	Bottom dead centre		**mpg**	Miles per gallon
BMEP	Brake mean effective pressure		**MSP**	Multi-side port
BSFC	Brake specific fuel consumption		**NEDC**	New European drive cycle
BTDC	Before top dead centre		**NOx**	Oxides of nitrogen
CAC	Charge air cooler		**PFI**	Port-fuel injection
CO	Carbon monoxide		**R**	Generating radius (of the geometry)
CR	Compression ratio		**REx**	Range extender
DCEE	Double compression-expansion engine		**RON**	Research octane number
DHICE	Dedicated Hybrid Internal Combustion Engine		**SI**	Spark ignition
e	Generating eccentricity (of the geometry)		**TDC**	Top dead centre
EMS	Engine management system		**THC**	Total hydrocarbons
EPC	Exhaust port closing		**TWC**	Three-way catalyst
EPO	Exhaust port opening		**ULG**	Unleaded gasoline
ER	Expansion ratio		**WLTC**	Worldwide light-duty test cycle
ESA	Eccentric shaft angle		**WOT**	Wide-open throttle
HC	Hydrocarbon			
HP	High pressure			
IPC	Intake port closing			
IPO	Intake port opening			
LP	Low pressure			

Appendix 1: Test equipment for Mazda 13B-MSP "RENESIS" engine dynamometer testing

For the Mazda 13B-MSP dynamometer measurements the test equipment and the fuel used is detailed below.

Dynamometer

David McClure 215 kW, 3 phase 415 V AC dynamometer. Maximum speed 9000 rpm, maximum water flow 25 l/min, maximum water temperature 30°C, and maximum water pressure 16 psi (1.1 bar).

Emissions equipment

Two Horiba MEXA 7000 series gas analyzers simultaneously performed the measurement of exhaust gases (HC, O_2, CO_2, CO and NOx) before and after the catalytic converter. From these two measurements the catalyst conversion efficiency was calculated as shown in the main body of the paper.

Sensors

The sensor types are detailed in Table A1.1.

Table A1.1: Sensors used in testing the Mazda 13B-MSP "RENESIS" twin-rotor engine

Parameter	Transducer Type	Operating Range	Accuracy
All temperatures	K type thermocouples	-180 to 1350°C	±0.75%
Fuel mass flow rate	Emerson Coriolis Micro motion CMF010M	9357 kg/hr nominal	Less than 0.1% above 2 kg/hr
Oil mass flow rate	Krohne Coriolis Optimass 6400C	Maximum 3800 kg/hr	±0.05%

Air mass flow rate was calculated using the fuel mass flow rate and the AFR (calculated from emission gases using the carbon balance method).

Fuel

The fuel used was a Euro 6 grade E10 ULG complying with EN228 (this being the same fuel used for testing the RX8 vehicle with this engine fitted on the chassis dynamometer, as reported in [1]). The stoichiometric AFR of this fuel was 13.922 and its full specification is given in Table A1.2.

Table A1.2: Fuel specifications for dynamometer testing of Mazda 13B-MSP Rotary Engine

10/19/2016

Test	Method	Unit	Limit Min	Limit Max	Result
Appearance	Visual		Report		C&B
Appearance @ -7°C	Visual		Report		C&B
RON	EN ISO 5164		95.0	98.0	95.9
MON	EN ISO 5163		85.0	89.0	85.5
Density @ 15°C	EN ISO 12185	kg/L	0.7430	0.7560	0.7494
DVPE @ 37.8°C	EN 13016-1	kPa	56.0	60.0	57.5
Sulfur	EN ISO 20846	mg/kg	-	10.0	2.1
Water Content	EN ISO 12937	mg/kg	-	0.050	0.031
Aromatics	ASTM D1319	% v/v	Report		27.9
Olefins	ASTM D1319	% v/v	Report		8.9
Saturates	ASTM D1319	% v/v	Report		53.4
PIONA					
Paraffins	EN ISO 22854	% v/v	Report		46.1
Olefins	EN ISO 22854	% v/v	6.0	13.0	8.4
Naphthenes	EN ISO 22854	% v/v	Report		5.7
Aromatics	EN ISO 22854	% v/v	25.0	32.0	30.2
Benzene	EN ISO 22854	% v/v	-	1.00	0.1
Oxygenates					
Methanol	EN ISO 22854	% v/v	Report		<0.1
Ethanol	EN ISO 22854	% v/v	9.0	10.0	9.5
MTBE	EN ISO 22854	% v/v	Report		<0.1
ETBE	EN ISO 22854	% v/v	Report		<0.1
Other	EN ISO 22854	% v/v	Report		<0.1
Oxygenates - Total	EN ISO 22854	% v/v	Report		9.5
Oxidation Stability	EN ISO 7536	min	480	-	>480
Copper Corrosion (3h at 50°C)	EN ISO 2160	Rating	Class 1	-	1A
Existent Gum - Washed	EN ISO 6246	mg/100mL	-	4	<1
Lead	EN 237	mg/L	-	5.0	<2.5
Phosphorus	ASTM D3231	mg/L	-	1.30	<0.20
Carbon	EN ISO 22854	% m/m	Report		83.34
Hydrogen	EN ISO 22854	% m/m	Report		13.16
Oxygen	EN ISO 22854	% m/m	3.30	3.70	3.50
C/H Mole Ratio	Calculation		Report		0.53
C/O Mole Ratio	Calculation		Report		31.72
Gross Calorific Value	ASTM D3338 mod	MJ/kg	Report		44.06
Net Calorific Value	ASTM D3338	MJ/kg	Report		41.27

Oil

Mazda Dexelia Ultra 5W/30 fully-synthetic oil, obtained from the local Mazda dealer.

10/19/2016

Appendix 2: Catalysts efficiency maps obtained from Mazda 13B-MSP "RENESIS" engine dynamometer testing

The measured efficiencies of the TWC are given in Figures A2.1, A2.2, and A2.3 for HC, CO, and NOx respectively. As mentioned above, the engine avoids enrichment at WOT up to relatively high speeds, and this is reflected in the high catalyst efficiencies up to this point.
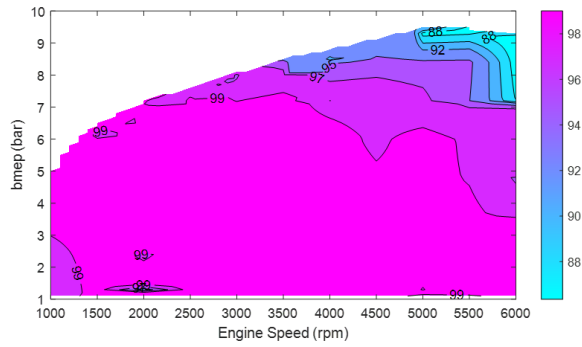

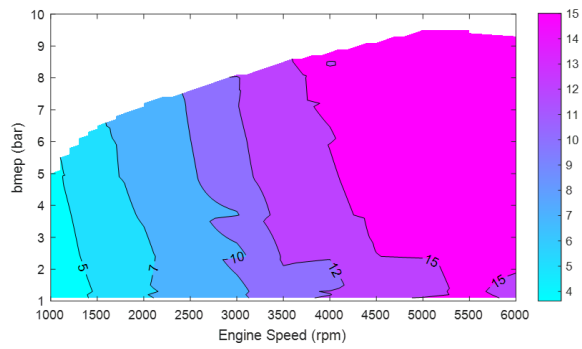Fig. A2.1: Measured catalyst HC efficiency map (in %) for Mazda 13B-MSP twin-rotor engine

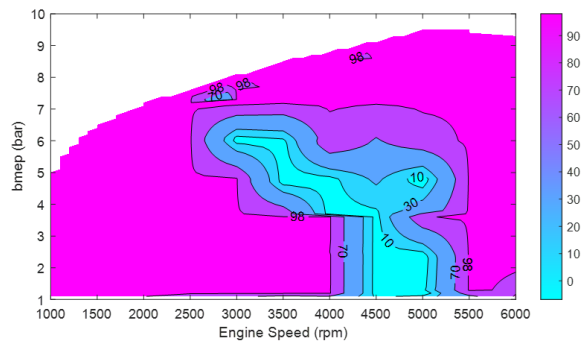Fig. A2.2: Measured catalyst CO efficiency map (in %) for Mazda 13B-MSP twin-rotor engine

Fig. A2.3: Measured catalyst NOx efficiency map (in %) for Mazda 13B-MSP twin-rotor engine

10/19/2016

Appendix 3: Coolant and oil specific heat capacity relationships for Mazda 13B-MSP "RENESIS" Engine Testing

Coolant

Ethylene glycol, 50:50 v/v in water

Specific heat capacity (J/kg/K) = (0.0033*T_coolant_av+3.3195) *1000

Density (kg/m^3) = (-0.0003*T_coolant_av+1.1001) *1000

Where T_coolant_av is the average of the coolant temperatures into and out of the engine.

Oil

Heat capacity (J/kg/K) = (3.8xToilavg+ 1925)

Where Toilavg is the average of the oil temperatures into and out of the engine.

10/19/2016

Appendix 4: Rotor chamber data for intake and exhaust port timing parametric investigations

Table A4.1: Intake port timing investigated as part of parametric study. Compression and expansion ratios stated are trapped values. Negative EPC values are degrees before TDC

Parameter	Baseline Condition	Zero Overlap Condition	Zero Overlap IPC-20°	Zero Overlap IPC-40°	Zero Overlap IPC-60°	Zero Overlap IPC-80°	Zero Overlap IPC-100°
IPO (°BTDC)	71	7	7	7	7	7	7
IPC (°ABDC	60	124	104	84	64	44	24
Duration (°ESA)	401	401	381	361	341	321	301
Chamber volume @ IPC (litres)	0.223	0.152	0.177	0.200	0.220	0.235	0.245
Trapped CR (:1)	8.50	5.79	6.75	7.62	8.37	8.95	9.33
EPO (°BBDC)	69	133	133	133	133	133	133
EPC (°ATDC)	57	-7	-7	-7	-7	-7	-7
Duration (°ESA)	396	396	396	396	396	396	396
Chamber volume @ EPO (litres)	0.216	0.141	0.141	0.141	0.141	0.141	0.141
Trapped ER (:1)	8.20	5.35	5.35	5.35	5.35	5.35	5.35
ER/CR	0.96	0.92	0.79	0.70	0.64	0.60	0.57

Table A4.2: Exhaust port timing investigated as part of parametric study. Compression and expansion ratios stated are trapped values. Negative EPC values are degrees before TDC

Parameter	Baseline Condition	Zero Overlap Condition	Zero Overlap IPC-20°	Zero Overlap IPC-40°	Zero Overlap IPC-60°	Zero Overlap IPC-80°	Zero Overlap IPC-100°
IPO (°BTDC)	71	7	7	7	7	7	7
IPC (°ABDC)	60	124	124	124	124	124	124
Duration (°ESA)	401	401	401	401	401	401	401
Chamber volume @ IPC (litres)	0.223	0.152	0.152	0.152	0.152	0.152	0.152
Trapped CR (:1)	8.50	5.79	5.79	5.79	5.79	5.79	5.79
EPO (°BBDC)	69	133	113	93	73	53	33
EPC (°ATDC)	57	-7	-7	-7	-7	-7	-7
Duration (°ESA)	396	396	376	356	336	316	296
Chamber volume @ EPO (litres)	0.216	0.141	0.166	0.190	0.212	0.229	0.241
Trapped ER (:1)	8.20	5.35	6.32	7.24	8.05	8.71	9.19
ER/CR	0.96	0.92	1.09	1.25	1.39	1.50	1.59

10/19/2016